Drag and instability of a free-falling cylinder in varying boiling regimes and with varying surface topographies

Journal Pre-proof

drag and instability of a free-falling cylinder in varying boiling regimes and with varying surface topographies

Adrian Jonas, Daniel Orejon, Khellil Sefiane

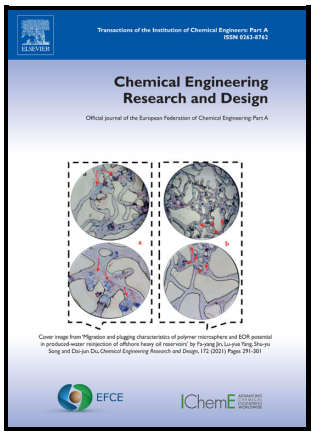

PII: S0263-8762(23)00097-7

DOI: https://doi.org/10.1016/j.cherd.2023.02.034

Reference: CHERD5469

To appear in: *Chemical Engineering Research and Design*

Received date: 28 September 2022
Revised date: 22 December 2022
Accepted date: 20 February 2023

Please cite this article as: Adrian Jonas, Daniel Orejon and Khellil Sefiane, drag and instability of a free-falling cylinder in varying boiling regimes and with varying surface topographies, *Chemical Engineering Research and Design,* (2022) doi:https://doi.org/10.1016/j.cherd.2023.02.034

DRAG AND INSTABILITY OF A FREE-FALLING CYLINDER IN VARYING BOILING REGIMES AND WITH VARYING SURFACE TOPOGRAPHIES

Adrian Jonas[a], Daniel Orejon[a], and Khellil Sefiane[a]*

[a] Institute for Multiscale Thermofluids, School of Engineering, University of Edinburgh, Edinburgh EH9 3FD, United Kingdom.

*Address correspondence to Prof. Khellil Sefiane, School of Engineering, University of Edinburgh, Edinburgh, United Kingdom. E-mail: K.Sefiane@ed.ac.uk

Abstract

This paper presents an experimental investigation regarding the drag and instabilities involved in free-falling cylinders across different boiling regimes. We aim to identify the mechanisms that cause the instabilities as well as to quantify the strength of these forces for temperatures between 25^{o}C and 550^{o}C. Understanding the forces involved across boiling regimes is essential when designing sensitive instruments, such as microelectronic devices. Cylinders with sizes in the range of tens of millimetres are released into a vertical column filled with Novec 7000. The surface of the cylinders were engraved with various patterns and experiments were conducted to investigate 10 topological designs, and bored-out hollows within the cylinders forced vertical free-fall. The control cylinders were smooth, while the others had ratchet teeth engraved on their surface. Ratcheted cylinders were manufactured in pairs to compare ratchet directionality to identify the action of self-propulsion due to viscous friction. We find that in two-phase (solid-liquid) free-fall, the liquid flow path over the solid surface dominates the cylinder behaviour. We categorise three-phase free-fall by the nucleate and film boiling regimes. For cylinders that free-fall under the nucleate boiling regime, random nucleate boiling action cause cylinders' instabilities, while

cylinders free-falling under the film boiling regime are stable due to a clear separation between the solid and liquid interfaces. We thus introduce viscous friction as an important parameter within three-phase systems.

Keywords:

Leidenfrost; Vapour Flows; Self-Propulsion; interfacial phenomena; Drag; Instability

1. Introduction

When Johann Gottlob Leidenfrost placed water in the bowl of a glowing hot spoon circa 1756 the water did not immediately evaporate [1]. Instead, the water levitated and became insulated by a thin film of vapour, separating the water from the glowing spoon. We know today that a minimum heat flux exists, since dubbed the Leidenfrost point, beyond which a heated liquid will be separated from a heat source, be it pool or plate, by the evaporate of the heat sink [2, 3]. A similar effect is noticed for the case of sublimation where the sublimate of a solid will levitate and insulate sublimating objects [4, 5]. The separation achieved between heat source and sink develops a lubricated environment where the motion of these levitating liquid droplets and solid components are virtually frictionless. Stationary Leidenfrost articles, which we define as a system or material where one of the phases undergoes a phase-change, can evaporate or sublimate symmetrically [6]. More typically the Leidenfrost effect results in seemingly random motion. This motion, now known as self-propulsion, occurs due to topographical asymmetries in either the heat source or sink which cause asymmetric vapour expulsion [7, 8, 9]. By designing asymmetric structures within a heat source or sink, such as a ratcheted plate, the motion of a Leidenfrost article can be controlled. Linke *et al*. [7] directed liquid droplets using ratcheted surfaces and found that droplets would move "*backwards*" if compared to the traditional operation of a gear and pawl mechanism. Several mechanisms have been proposed to explain this unintuitive result including

Marangoni flows [10], vapour flows induced by thermal creep [11], jet thrusts [4], and vapour rectification [7, 12]. Self-propulsion based on viscous friction, which is the most widely studied mechanism, has been used to explain both the motion of solids and liquids [13]. Experimental observations [14] have been corroborated with numerical [15] and analytical models [9] to show that asymmetries direct the vapour flow. Self-propulsion of evaporating liquids and sublimating solids occur on various textured substrates including; ratchets [16], herringbones [12], and asymmetric microstructures [17]. Self-propulsion can be utilised to convert thermal energy to mechanical or electrical work by taking advantage of the translation [15, 18, 19] or rotation [20] of these objects. Effectively, the Leidenfrost effect can be used as the mechanism to drive torque transfer from an active substance to solid components to form a mechanical heat engine. Wells *et al*. [20] demonstrated a sublimation driven heat engine using dry-ice rotation on turbine-like substrates suggesting the potential for such a device to provide an energy resource in deep space exploration expeditions, while droplets using the Leidenfrost effect have produced a net torque to suggest the potential for energy production in microelectronic devices [13]. An interesting parallel to the Leidenfrost effect is supercavitation. While the Leidenfrost effect address vapour produced by a temperature difference, supercavitation address vapour produced by pressure differences. When a fluid flows over a bluff body in a stream, the fluid flow over the body's surface increases in velocity, and under the right conditions, conservation of energy reduces the flow pressure surrounding the body to cause the phase change. Like in the case of the Leidenfrost effect, the resulting three-phase system almost eliminates skin friction drag causing submerged bodies to achieve extremely high speeds [21–24]. Supercavitation has been implemented through the Shkval torpedo which could travel through water at more than 100 m/s [25]. Vakarelski *et al*. [26] demonstrated the parallels between these two physical mechanisms by showing drag reduction caused by the Leidenfrost effect. Superheated spheres would increase turbulence within the vapour layer, delaying the flow separation of the wake and reducing the

drag coefficient. The literature suggests promising applications of vapour separation between solid bodies and working liquids; however, fundamental questions regarding the unstable nature of boiling remain open. Between the two regions of stability lies a poorly defined region of instability which we aim to describe and explain using the Euler Angles of falling cylinders. The traditional view is that the free-fall of cylinders is largely dependent on initial drop angle, body aspect ratio, and mass centre [27]. We propose that the viscous effect is more dominant than previously thought, as when changed through the introduction of vapour, an initially unstable cylinder can become stable. Furthermore, the action of cavitating bubbles, produced by either a pressure or temperature difference, near the surface of a cylinder can destabilise an initially stable cylinder. Lagubeau *et al*. [4] reported the self-propelling viscous drag force to be in the order of μN. Therefore, ratchets with lengths in the millimetre range and heights in the submillimetre range engraved along the length of the cylinders would maximize the chances of observing self-propulsion. Chu *et al*. [28] reported that a cylinder would fall vertically by separating the centre of mass (CoM) from the centre of volume (CoV) , where χ is COV – COM, in a moderately dense fluid.

2. Experimental

We hollow the cylinders out by analysing the drag forces on either side of the centre of gravity (CoG) to give a hollow 62.5% the cylinders length and 80 - 85% its diameter (Table 1). In hollowing the cylinders, the thermal energy any given cylinder can store is also reduced. To maximize the probability of achieving the Leidenfrost effect for a sufficient period for a cylinder to reach terminal velocity, we chose aluminium with a significantly high specific heat capacity among common metals but with a low enough density as to reach terminal velocity within our column. Manufacturing ratchets into aluminium cylinders at this scale is technically challenging, resulting in imperfect ratchet structures, especially for ratchets with teeth of lengths between 1 – 1.1 mm. With aluminium's melting point at ~600^{o}C, our experimental temperature

maximum was limited to 550^{o}C to avoid unintentional tampering of the ratchet structures. Cylinders were individually released to fall freely in an extruded acrylic square tube column, 1500mm in length and 75mm in width and depth. A backing light 1000mm in length was used to provide contrast to the falling cylinders. Experimental data was captured between depths of 9mm - 90mm. A guiding release shoot controlled the initial drop angle, also ensuring true free-fall occurred only once the cylinders were submerged (Figure 1). The guiding shoot is immersed 3 mm into the fluid and the object is released from 7 mm above the liquid interface. We use 3M™ Novec™ 7000 Engineered Fluid, which is a clear, colourless, thermally stable dielectric fluid.

Table 1. Dimensions of cylinder design used within this experimental investigation. *D*: cylinder diameter (±0.3 mm), *d*: hollow diameter (±0.3 mm), *L*: cylinder length (±0.3 mm), *l*: hollow depth (±0.3 mm), *P*: pitch height (±0.3 mm), *h*: ratchet height, *w*: ratchet width.

Label	Ratchet Description	*D* (mm)	*d* (mm)	*L* (mm)	*l* (mm)	*P* (mm)	*h* (mm)	*w* (mm)	*h*/*w*
SC1	No ratchets	10	8.5	40	27	3	N/A	0	N/A
SC2	No ratchets	10.5	8.0	40	27	3	N/A	0	N/A
2.0LD	Lateral ratchets facing down	10	8.0	40	27	3	1	0.5	2.0
2.0LU	Lateral ratchets facing up	10	8.0	40	27	3	1	0.5	2.0
2.0SD	Spiral ratchets facing down	10	8.0	40	27	3	1	0.5	2.0
2.0SU	Spiral ratchets facing up	10	8.0	40	27	3	1	0.5	2.0
2.2LD	Lateral ratchets facing down	10	8.5	40	27	3	1.1	0.5	2.2
2.2LU	Lateral ratchets facing up	10	8.5	40	27	3	1.1	0.5	2.2
11.4LD	Lateral ratchets facing down	10	8.5	40	27	3	5.7	0.5	11.4
11.4LU	Lateral ratchets facing up	10	8.5	40	27	3	5.7	0.5	11.4

The relatively similar density of Novec 7000 when compared to the hollowed aluminium cylinders (**Table 2**) allows relatively stable free-falls using ratcheted aluminium cylinders and the low boiling point allows a range of boiling regimes. Data was captured at 1000 fps using a High Speed Camera (HSC)

Chronos 2.1-HD and a wide-angle lens to cover the entire 1500mm of free-fall, though our experiment was limited by the length of the 1000mm strip which provided the contrast required.

2.1. Methodology

Seven cylinder temperatures were explored (ambient [recorded as 23 ± 3 ^{o}C], 50^{o}C, 150 ^{o}C, 250 ^{o}C, 350 ^{o}C, 450 ^{o}C, and 550 ^{o}C). Cylinders were released one after the other in the following order, SC1, 2.2LU, 2.2LD, 11.4LU, 11.4 LD, SC2, 2.0LU, 2.0LD, 2.0SU, 2.0SD, allowing the cylinders to reach the bottom before releasing a subsequent cylinder Each cylinder was released and then extracted using the extraction unit depicted in Figure 1. After each extraction, the fluid level was inspected and topped up as necessary. K-type thermocouples, calibrated using a standard laboratory thermometer, were used to monitor the temperature of the pool. The experiment consisted of first heating the cylinders in an electric oven (Efco Enameling Kiln 180 KF) controlled by a PID controlled (Efco Temperature Controller TRP008 – Digital) before removing them with the help of metal forge pincers and releasing them to fall into the column. Existing software which could process the HSC footage led to significant errors and experimental noise. Therefore, we present a bespoke software tool (Moxie Analyser) that can find a moving object within a

Table 2. Relevant heat transfer properties for substances used within these experiments. Properties of given at ambient temperature and ambient pressure [29, 30].

Description	Density	Boiling/Melting Point	Viscosity	Latent Heat	Specific Heat Capacity	Thermal Conductivity
	(kg/m^3)	(^{o}C)	(cSt)	(kJ/kg)	(J/kg K)	(W/m K)
Aluminium (s)	2699	660	-	-	900	237
Novec7000 (l)	1400	34	0.32	142	1300	0.075

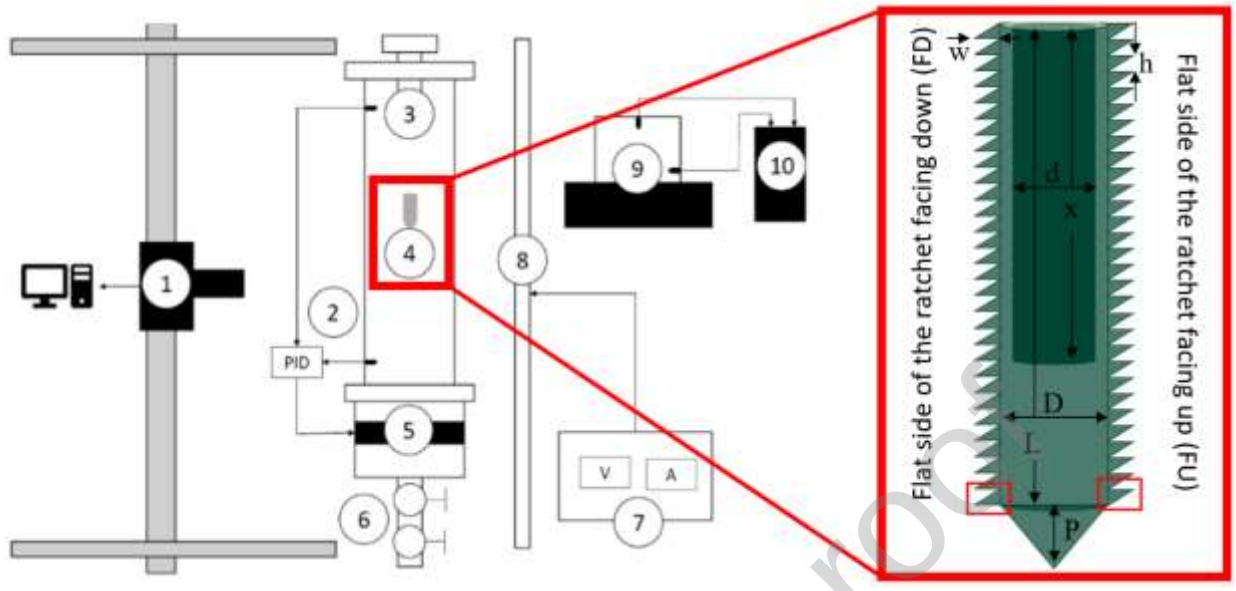

Sketch of 2.0SU **Sketch of 2.0LU or 2.2LU** **Sketch of 11.4LU**

Spiralled ratchets provide a flow path for vapour to escape

Lateral ratchets blocks flow path forcing flow over the ratchets

Increasing ratchet aspect ratio causes less flow disruption

Spiralled Set **Comparison of Hollows** **Aspect Ratio Set (2.2 and 11.4)**

Figure 1: The experimental schematic is shown at the top of the figure, where (1)-Chronos 2.1 HSC, (2)-Temperature Control, (3)-Guiding Release Shoot, (4)-Cylinder, (5)-Heater, (6)-Extraction Unit, (7)-Power Supply, (8)-Strip Light, (9)-Oven, (10)-Controller. Also shown are sketches and photos of the cylinder used in the experiment to illustrate the ratchet structures. .

video, track its position, and calculate physical parameters. **Error! Reference source not found.** shows the initial (**Error! Reference source not found.**a) and final (**Error! Reference source not found.**b) frames used to calibrate the Moxie Analyser for a free-falling smooth cylinder heated to 550^{o}C. The Moxie Analyser requires the experimentalist to insert spatial measurements used as calibration points to convert pixels to distance values. The frame rate defines the experiment's time acquisition, and important physical parameters are calculated with distance-time relations. An HSC decreases the time between each data acquisition, increasing the accuracy of the calculated parameters. The tracking tool also produces a processed image (**Error! Reference source not found.**d) from the original captured footage (**Error! Reference source not found.**c), which shows the experimentalist the free-fall trajectory and provisional vapour layer thickness (**Error! Reference source not found.** and **Error! Reference source not found.**). Raw data overlapped by data produced from a robust quadratic regression algorithm built within MATLAB removes noise from the results. Experimental iterations identify random errors and time errors comes from the frame rate used to capture the data. Table 2 shows the physical properties of the materials used within our experiment. Uncertainty in the measurement of depth was calculated using the initial and final frames presented by **Error! Reference source not found.**(a-b), defined as ± 0.005 m in most cases. The typical distance covered by measurements was 0.83 m giving a typical relative uncertainty of 1%. The camera captures images at a 1000 ± 0.005 fps, which given that a typical experiment lasted 2 seconds, results in a negligible relative error of 0.00005%. Using the calculated relative errors in measurement, we calculate an absolute error in space (x, y) and time (t) for each frame where the cylinder was observed. A regression was preformed using the data captured from five experimental iterations. After calculating the absolute velocity errors, the residual errors taken from the regression were added. Five repeated experiments help identify the random errors, giving an area of uncertainty around the regression lines.

2.1.1. Uncertainties

Equation 1 applies "the propagation of errors" to define the errors associated to the free-fall path length.

$$\sigma_{Pl} = \left(\frac{dPl}{dx}\right)_y^2 \sigma_x^2 + \left(\frac{dPl}{dy}\right)_x^2 \sigma_y^2 \ \#(1)$$

Where σ_{Pl} is the absolute error in pathlength, $\frac{dPl}{dx}$ is the magnitude of pathlength associated with a change in x-position, σ_x is the absolute error associated with the change in x-position, $\frac{dPl}{dy}$ is the magnitude of pathlength associated with a change in y-position, σ_y is the absolute error associated with the change in y-position. The relative error associated with path length was then calculated, which was used to calculate the relative error associated with each calculated velocity value.

3. Results

We propose that the mechanism with which the fluid interacts with the cylinders as they fall is dependent on whether the single phase, nucleate boiling, and/or film boiling regimes ensues. In the single-phase regime, two phases are present – solid, in the form of the aluminium cylinder and liquid, in the form of liquid Novec 7000. In the nucleate boiling regime, three phases are present – solid and liquid as before with vapour, in the form of bubbles of vaporised Novec 7000. For the film boiling regime, there are also three phases present - solid and liquid phase present as in the former two cases; however, a distinctive layer of vaporised Novec 7000 clearly separating the two phase boundaries i.e., the solid-vapour interface and the liquid-vapour interface. Categorizations are based on the boiling regimes observed at the terminal velocity which does not imply a single regime was observed throughout the fall. Single phase experiments consisted of cylinders released at isothermal conditions and cylinders released after being initially heated to 50℃. Nucleate boiling experiments consisted of initially heated cylinders to 150℃ and

250℃. Film boiling experiments consisted of initially heated cylinders to 350℃, 450℃, and 550℃. Nucleate boiling was more violent and unstable, while film boiling experiments were smoother. This means, for nucleate boiling runs

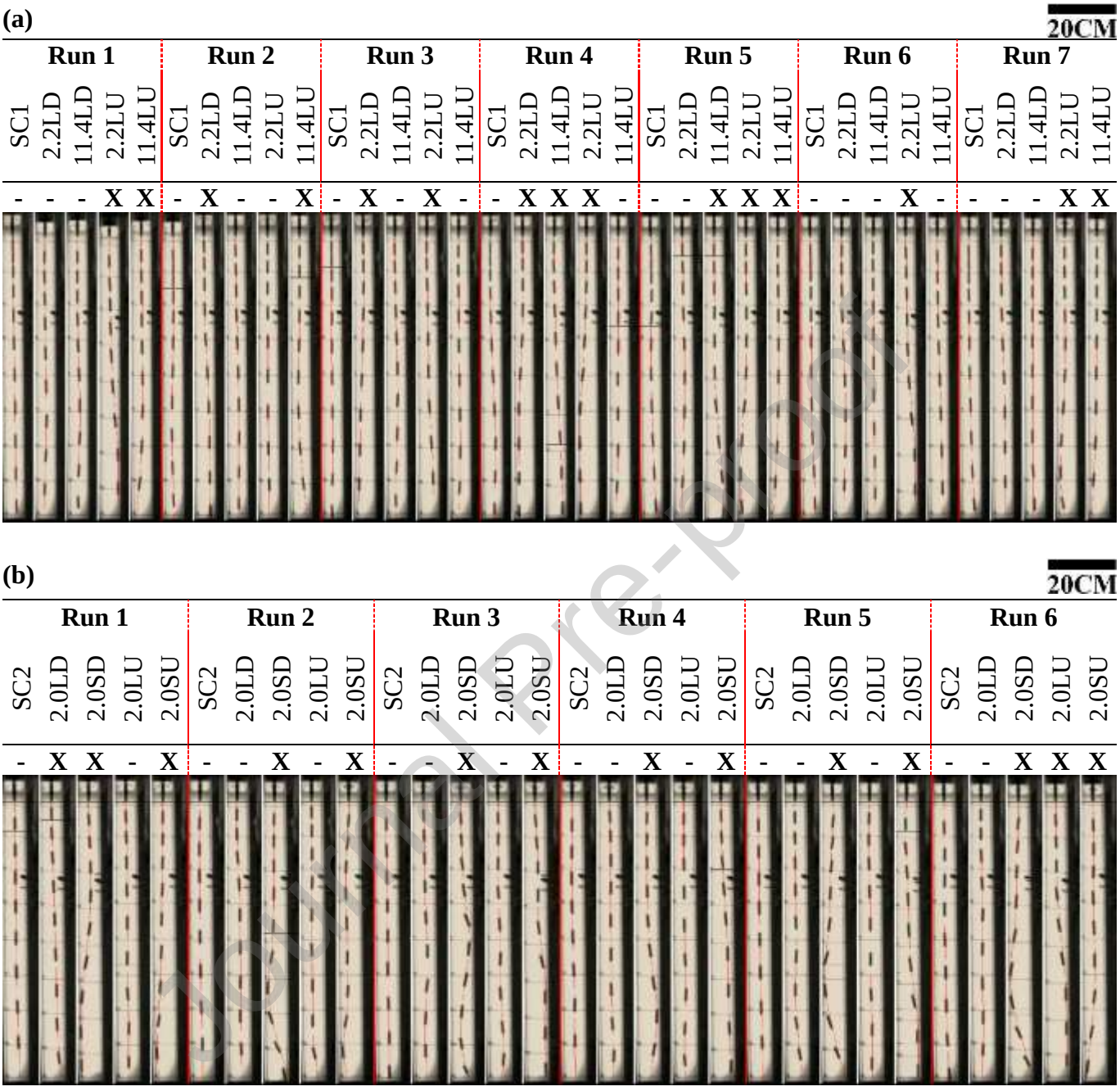

Figure 2: Trajectories of free-falling cylinders at isothermal conditions. Downward facing ratchets are more stable than upward facing ratchets. Stability decreases with decreasing aspect ratio. Spiralling ratchets significantly disrupt stability in this regime. X symbol denotes the cylinder hitting the wall.

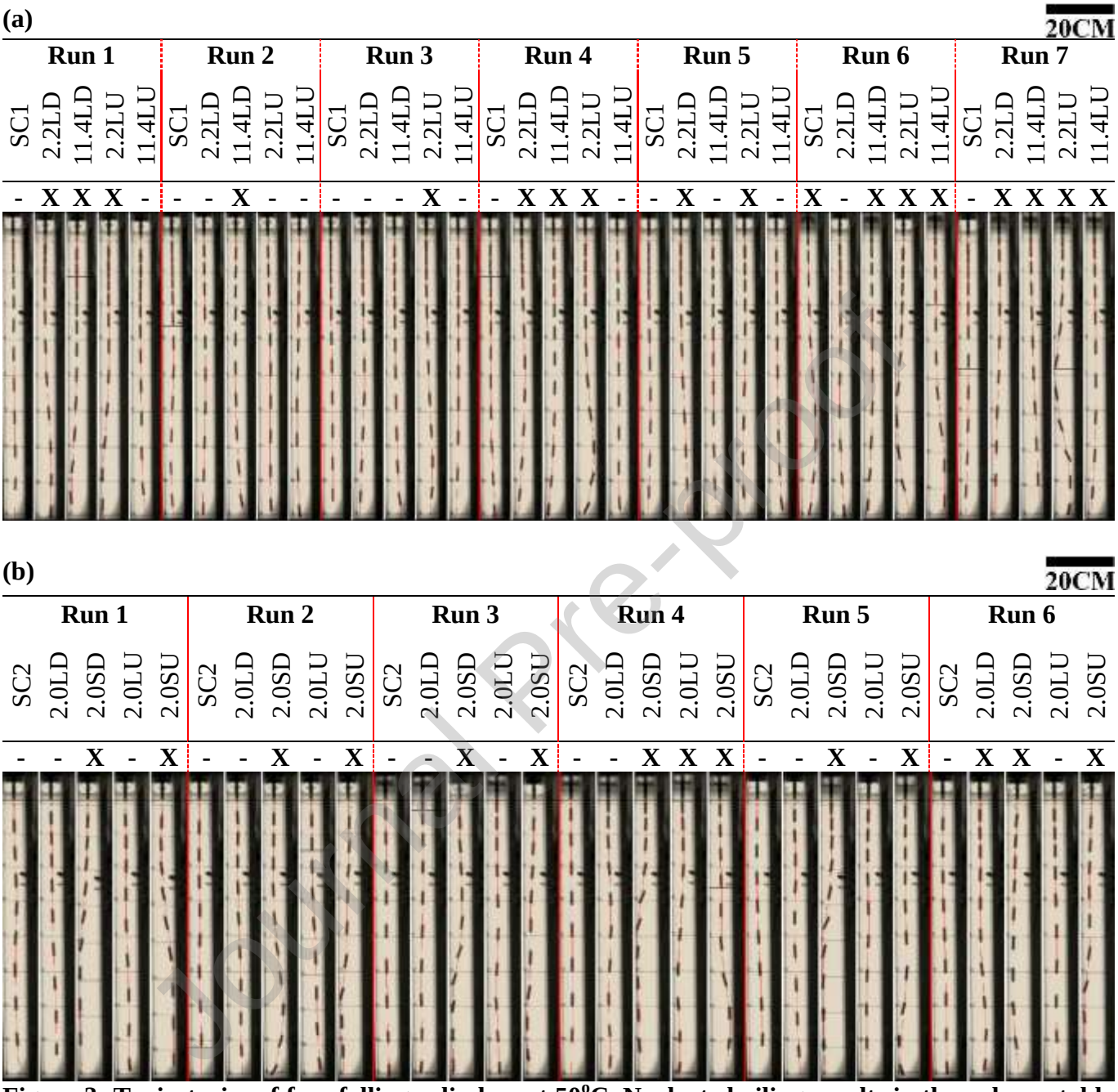

Figure 3: Trajectories of free-falling cylinders at 50°C. Nucleate boiling results in the only unstable smooth cylinder and spiralling disrupts stability. For AR 2.2, downward facing ratchets are more stable but for AR 11.4 upward facing ratchets are more stable. X symbol denotes the cylinder hitting the wall.

one could hear the boiling and one could visually see the regime. For the film boiling experiments, there was significantly less auditory noise, and one could see the glint of a vapour film as the cylinders fell. Control cylinders (SC1 and SC2) vary in CoM location caused by a difference in hollow diameter; however, the maximum deviation of CoM concerning all the cylinders is within 5.4%. The centre of mass is 9.30 mm and 9.81 mm from leading edge of the cylinder as it falls for SC1 and SC2 respectively. For ratcheted cylinders the CoM is 9.98 mm, 9.57 mm, and 9.73 mm from the cylinder base for aspect ratios of 2.0, 2.2, and 11.4 respectively. SC1 occupies 1.69 ml, compared to 2.18 ml for SC2. 2.0LD, 2.0LU, 2.0SD, and 2.0SU have a volume of 1.86 ml. 2.2LD, 2.2LU, 11.4LD, and 11.4LU all occupy 2.02 ml.

3.1. Single Phase

Figure 2 shows the trajectories of aluminium cylinders falling in Novec 7000 at isothermal conditions i.e., the fluid temperature and the cylinder temperature are both 25℃ ± 3℃. Figure 2a presents the experimental runs comparing the effects of ratchet aspect ratio on the stability of free-falling cylinders, while Figure 2b compares the stability of laterally orientated ratchets with ratchets that spiral upwards like a screw. Similarly, Figure 3 shows the trajectories of aluminium cylinders falling in Novec 7000 after the aluminium cylinders were initially heated to 50℃ ± 3℃. The pool remained at room temperature. The experiments within this section consider terminal velocities between 0.651 – 0.776 m/s, at depths of between 0.573 – 0.881 m. It takes between 0.90 – 1.50 s for cylinders falling within the single-phase to reach these depths and these terminal velocities, (v_t), see Table 3. It is clear that under single-phase conditions, spiralling the ratchet structures causes significant instability with no experiments completing a free-fall without colliding with the walls of the column, while 83% of cylinders with laterally orientated ratchet structures completed the free-fall. To a lesser extent reducing the aspect ratio (AR) decreases stability with a completion rate of 32% for cylinder with an AR of 2.2 and a completion rate of 54% for

cylinder with an AR of 11.4.

Table 3: A summary table with all the terminal velocities (±0.038 m/s), depths (±0.034 m), and times to reach the terminal velocity, (v_t), where cylinders were observed to fall within the single phase regime.

	Temp.	SC1	SC2	2.2LD	11.4LD	2.2LU	11.4LU	2.0LD	2.0SD	2.0LU	2.0SU
v_t (m/s)	25℃	0.708	0.728	0.743	0.713	0.757	0.767	0.703	0.660	0.721	0.718
	50℃	0.707	0.720	0.736	0.688	0.713	0.776	0.697	0.651	0.711	0.694
Depth (m)	25℃	0.637	0.881	0.642	0.679	0.705	0.720	0.573	0.616	0.587	0.656
	50℃	0.690	0.838	0.597	0.810	0.631	0.810	0.582	0.716	0.621	0.607
Time (s)	25℃	1.15	1.30	1.00	1.10	1.10	1.10	0.90	0.95	0.90	1.00
	50℃	1.50	1.20	1.10	1.40	1.15	1.45	0.95	1.20	1.00	0.95

3.2. Nucleate Boiling

Figure 4 shows the trajectories of aluminium cylinders falling in Novec 7000, which remained at room temperature (25 ± 3℃.), after being heated to 150℃ ± 3℃. Figure 4a presents the experimental runs comparing the effects of ratchet aspect ratio on the stability of free-falling cylinders, while Figure 4b compares the stability of laterally orientated ratchets with ratchets that spiral upwards like a screw. Similarly, Figure 5 shows the trajectories of aluminium cylinders after they were initially heated to 250℃ ± 3℃. Notably the cylinders in this section reach a lower terminal velocity and take longer to do so. Here cylinders fall slower with terminal velocities between 0.390 – 0.568 m/s, at similar depths of between 0.506 – 0.817 m, taking typically between 0.80 – 2.45 s to reach their respective terminal velocities – see Table 4. These observations suggest at the influence of the third less-dense vapour phase. In the nucleate boiling regime we see a significant dependence on AR as cylinders with an AR of 11.4 complete all of their free-falls without colliding with the column wall. Compare that to cylinders that have ARs of 2.2

where completion rates fall to 36%. Notably completion rates for these cylinders increased by 2% when compared to their single phase counterparts. In separating the data contained in Figure 4 from Figure 5, we see that

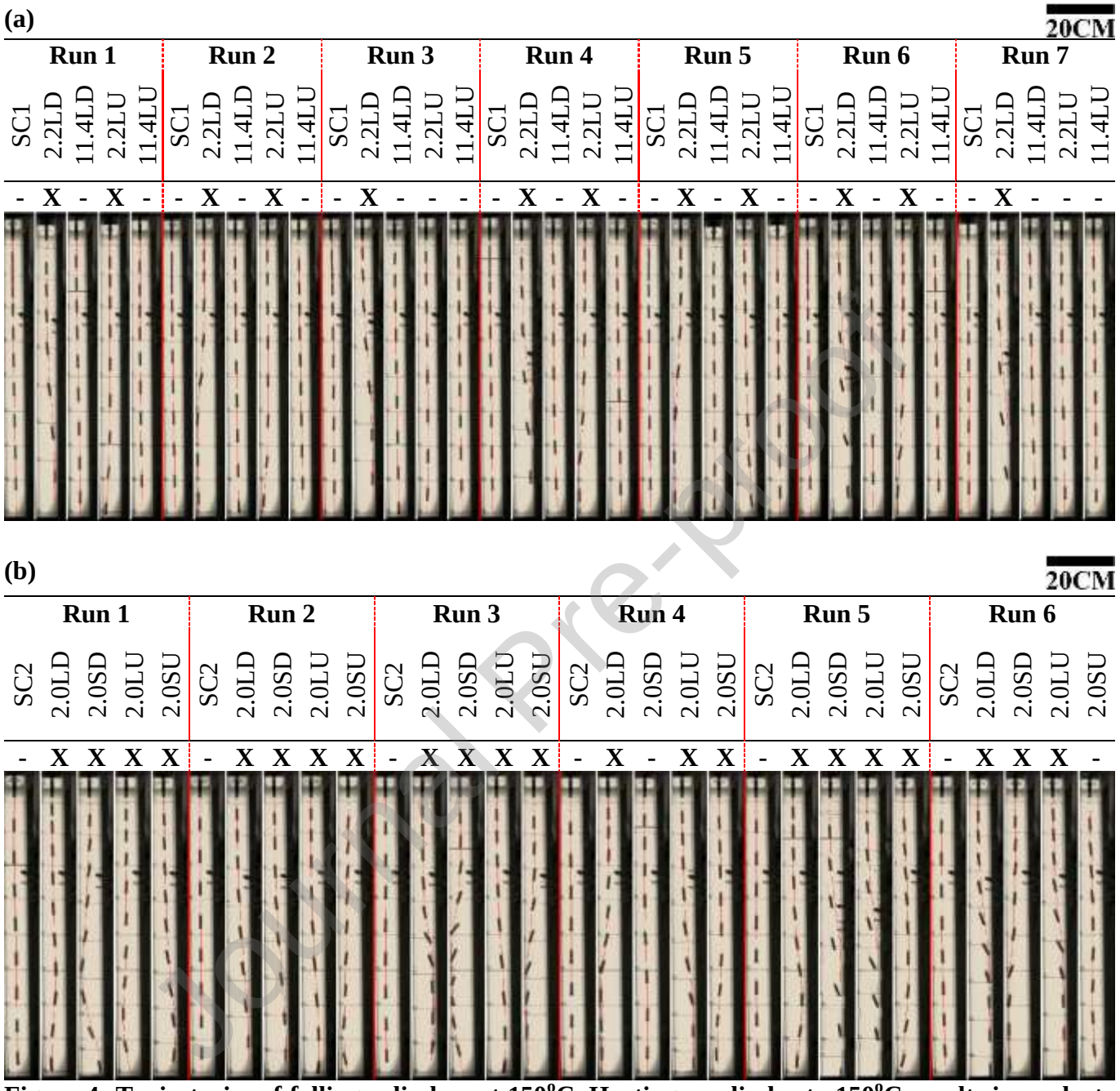

Figure 4: Trajectories of falling cylinders at 150°C. Heating a cylinder to 150°C results in nucleate boiling for ARs of 2.0 and 2.2. Nucleate boiling is delayed beyond the point of influencing stability for smooth cylinders and cylinders with an AR of 11.4. X symbol denotes the cylinder hitting the wall.

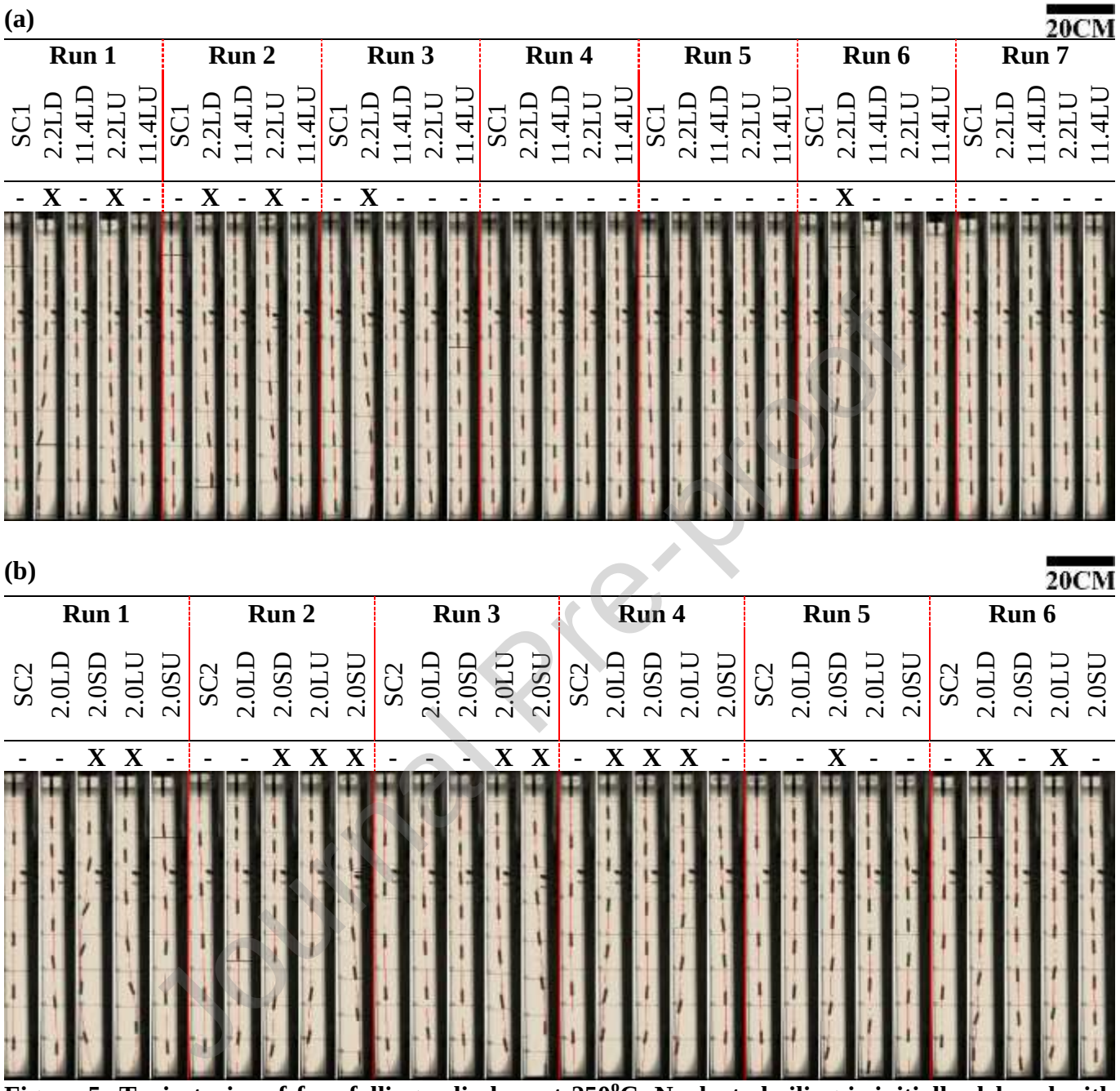

Figure 5: Trajectories of free-falling cylinders at 250°C. Nucleate boiling is initially delayed with the presence of film boiling at the onset. Larger surface areas lead to faster cooling where cylinders with AR 2.0 and 2.2 giveaway to nucleation instabilities. X symbol denotes the cylinder hitting the wall.

Table 4: A summary table with all the terminal velocities (±0.030 m/s), depths (±0.053 m), and times to reach the terminal velocity, (v_t), where cylinders were observed to fall within the nucleate boiling regime.

	Temp.	SC1	SC2	2.2LD	11.4LD	2.2LU	11.4LU	2.0LD	2.0SD	2.0LU	2.0SU
v_t (m/s)	150℃	0.431	0.523	0.544	0.503	0.566	0.446	0.499	0.568	0.550	0.545
	250℃	0.425	0.514	0.497	0.426	0.453	0.415	0.456	0.454	0.424	0.390
Depth (m)	150℃	0.595	0.506	0.766	0.727	0.699	0.808	0.779	0.690	0.528	0.822
	250℃	0.667	0.564	0.769	0.803	0.738	0.767	0.523	0.704	0.521	0.817
Time (s)	150℃	1.80	0.80	1.80	1.55	1.40	1.85	1.65	1.30	1.05	1.60
	250℃	2.45	0.95	2.15	2.25	1.95	2.10	1.40	1.80	1.35	2.05

only 14% of the experiments presented for a cylinder with an AR of 2.2, and initially heated to 150℃, fell without colliding with the column wall. These experiments have the lowest completion rates of the laterally orientated ratchets. From Run 3 in Figure 4a, we can see that cylinder 2.2LD would move away from its initial vertical position at a depth as shallow as 15cm, suggesting that instabilities arising from nucleate boiling have an influence from near the beginning of the free fall. If we compare the results in Figure 4 with the results in Figure 5 we see a marked increase in the overall completion rate from 33% to 62% - if you exclude the SC1 and SC2. Using cylinder 2.2LD as a bench mark, we can see from Run 6 in Figure 5a that the earliest deviations from vertical begin after 25cm. The observation from Figure 5 suggests that the cylinders are initially stable and begin to destabilise further down the column compared to their cooler counterparts implying the onset of nucleate boiling as the cylinders reach their terminal velocity – seen from Table 4. Another notable point is that within the nucleate boiling regime – spiralled ratchets become the more stable topography, with a completion of 33% compared to 21% for the laterally orientated counterparts. The stark difference between the results observed within the nucleate boiling regime and the single phase regime would suggest that the bubbles produced effectively decouple viscous

drag forces.

3.3. Film Boiling

Figure 6 shows the trajectories of aluminium cylinders falling in Novec 7000, which is at room temperature (25 ± 3 ℃), after initially heated to 350℃ ± 3℃. Figure 6a presents the experimental runs comparing the effects of ratchet aspect ratio on the stability of free-falling cylinders, while Figure 6b compares the stability of laterally orientated ratchets with ratchets that spiral upwards like a screw. Figure 7 shows the trajectories of aluminium cylinders falling in Novec 7000 after the aluminium cylinders were initially heated to 450℃ ± 3℃. The vapour film produced by the extreme temperature gradient known as the Leidenfrost effect dramatically reduces the terminal velocities of free-falling aluminium cylinders to between 0.251 – 0.478 m/s. The depths of these velocities are also dramatically less being achieved between 0.300 – 0.828 m, and as one might expect – the time taken to reach terminal velocity increase to between 0.95 – 6.45 s. It should be noted that these dramatic differences are mostly seen at a temperature of 550℃.

Table 5: A summary table with all the terminal velocities (±0.063 m/s), depths (±0.121 m), and times to reach the terminal velocity, (v_t), where cylinders were observed to fall within the film boiling regime.

	Temp.	SC1	SC2	2.2LD	11.4LD	2.2LU	11.4LU	2.0LD	2.0SD	2.0LU	2.0SU
v_t (m/s)	350℃	0.399	0.478	0.447	0.416	0.435	0.413	0.411	0.447	0.412	0.405
	450℃	0.369	0.438	0.377	0.343	0.398	0.366	0.367	0.354	0.380	0.337
	550℃	0.269	0.401	0.374	0.327	0.330	0.286	0.349	0.251	0.312	0.260
Depth (m)	350℃	0.682	0.627	0.549	0.764	0.707	0.781	0.525	0.735	0.562	0.819
	450℃	0.530	0.511	0.755	0.772	0.608	0.652	0.647	0.745	0.575	0.753

	550℃	0.489	0.593	0.646	0.398	0.300	0.728	0.828	0.620	0.760	0.723
Time (s)	350℃	2.70	1.15	1.85	2.35	2.05	2.35	1.55	2.05	1.60	2.25
	450℃	2.55	0.95	3.00	3.15	2.30	2.35	2.45	2.80	2.05	2.45
	550℃	3.95	1.25	5.30	3.05	2.65	4.05	6.45	4.20	4.25	3.65

For the terminal velocities, depths, and times to reach (v_t) for cylinders falling within the nucleate boiling regime – see Table 5. If we exclude cylinders SC1 and SC2, we can see from Figure 6 and Figure 5 that the completion rate for a cylinder initially heated to 350℃ is 57% compared to a cylinder initially heated to 250℃ at 62%. The result suggests the presence of viscous drag from the vapour layer separating the free-falling cylinder from the bulk fluid. Table 5 further demonstrates the result by revealing an average difference in terminal velocity between downward facing ratchets and upward facing ratchets of 0.014 m/s in favour of the downward facing ratchets when a cylinder is initially heated to 350℃. The average difference in terminal velocity between upward facing ratchets and downward facing ratchets within the single phase (Table 3) reveals that drag would resist the downward facing ratchets more than the upward facing ratchets. This result opposes the data within Table 4 and Table 5 suggesting further the presence of viscous drag action and therefore the possibility that viscous drag within the vapour layer causes the instabilities seen at 350℃. In combing the data presented with Figure 6, Figure 7, and Figure 8, we see that overall – the film boiling regime stabiles the spiralled ratchets to a greater extent than the lateral ratchets with completion rates of 92% and 67% respectively. We also notice that upward facing ratchets are more stable than downward facing ratchets with completion rates of 90% and 72% respectively. Zooming in (Figure A2 and Figure A3) and considering Figure 6, Figure 7, and Figure 8 individually we see more evidence for the presence of viscous drag within the vapour layer. When the vapour layer is thin, i.e., when the cylinders are initially heated to 350℃ we notice from Figure 6 that ratcheted cylinder have completion rates of 57%. Compare that to completion rates presented within Figure 7 and Figure 8 at 88% and 96% it is clear that as the vapour layer increases the stability of the

free-falls also increase. We also notice from Table 5 that terminal velocities for all ratcheted cylinders are relatively consistent and comparable; however, when we compare the times taken for ratcheted cylinders to reach terminal velocity we see significant variations, implying differences in surfaces temperatures and therefore vapour layer thickness.

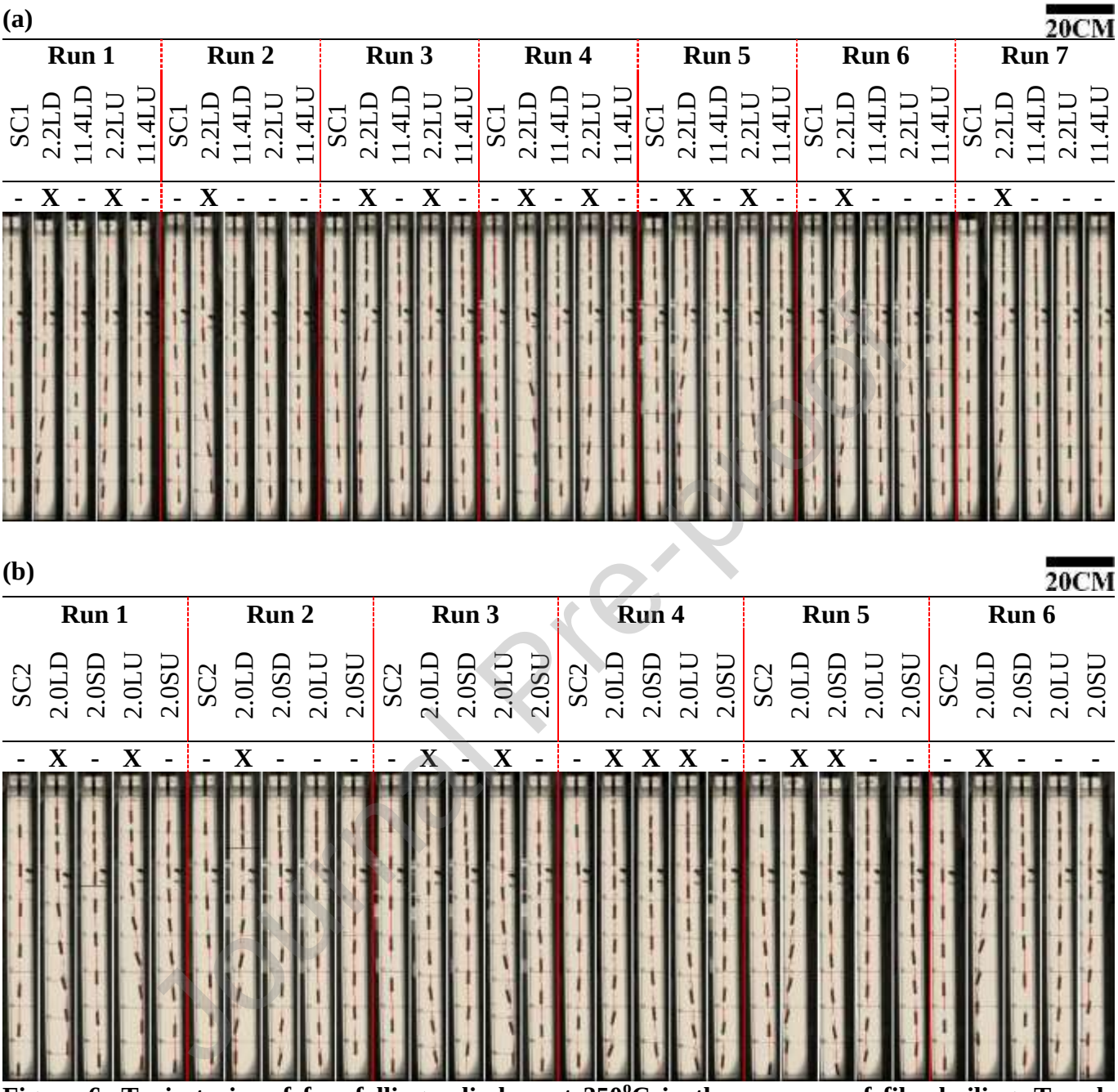

Figure 6: Trajectories of free-falling cylinders at 350°C in the presence of film boiling. Trends observed at isothermal conditions are here reversed. Spiralled cylinders are more stable and downward facing ratchets are less stable than upward facing ratchets. X symbol denotes the cylinder hitting the wall.

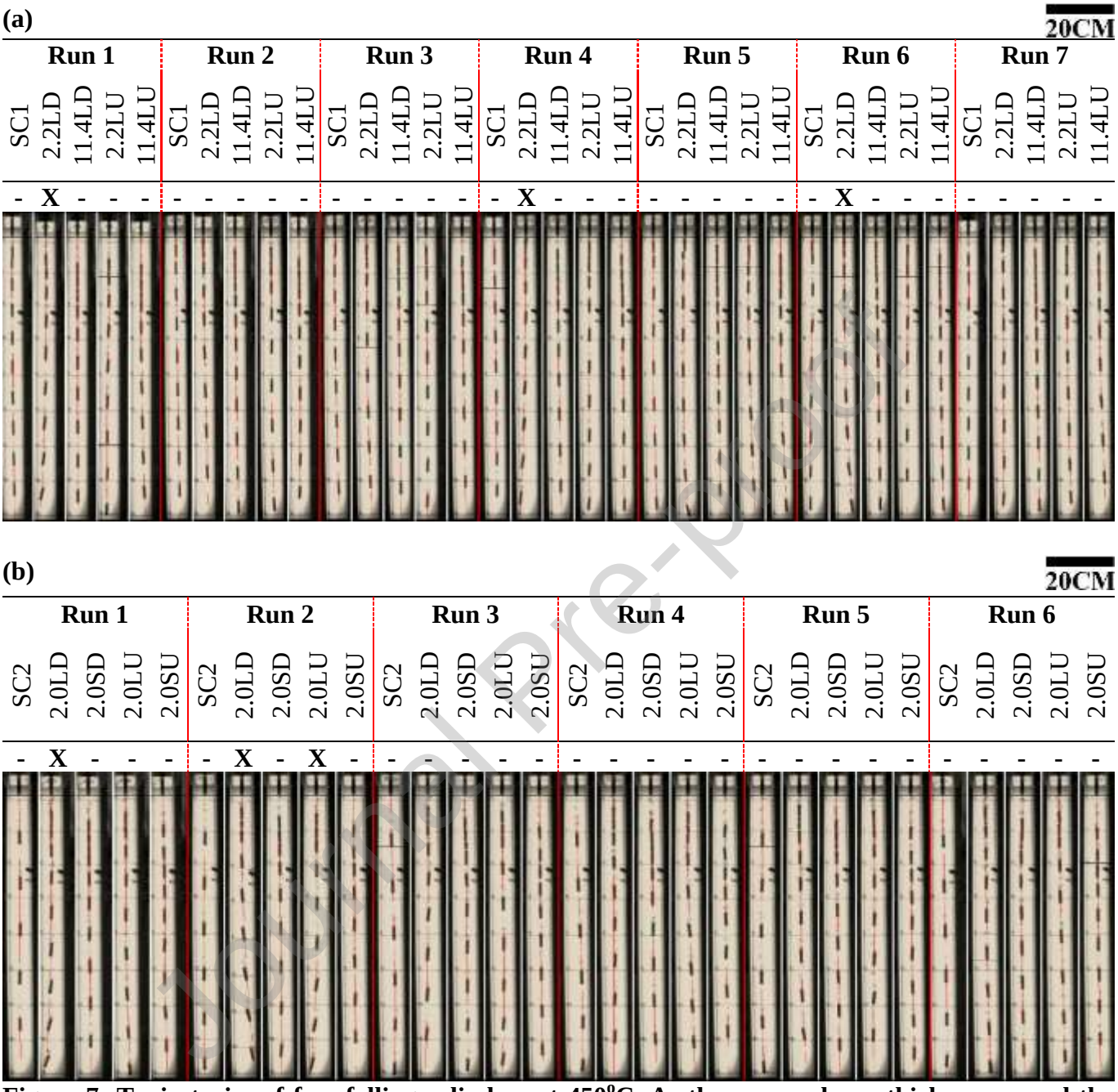

Figure 7: Trajectories of free-falling cylinders at 450°C. As the vapour layer thickens around the cylinders – topological difference in surface finish become increasingly irrelevant. Only cylinders 2.2LD, 2.0LD, and 2.0LU retain free-fall instabilities. X symbol denotes the cylinder hitting the wall.

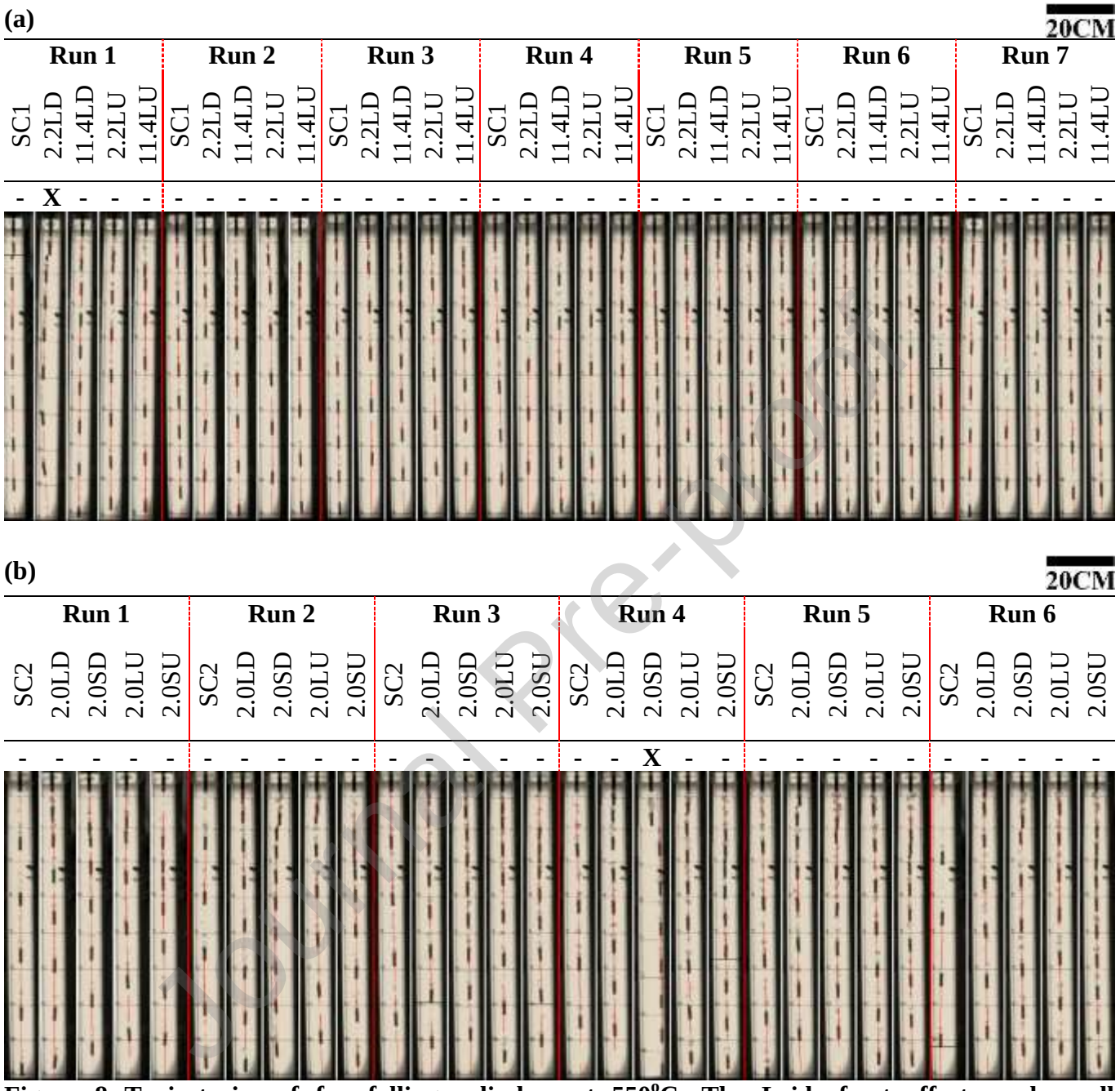

Figure 8 Trajectories of free-falling cylinders at 550°C. The Leidenfrost effect renders all topological differences to null. The apparent instability associated to 2.2LD and 2.0SD are due to viscous drag effects that pull the cylinders up and laterally. X symbol denotes the cylinder hitting the wall.

4. Analysis

The analysis is broken down into three sections: boiling regime classification, quantifying stability, and a discussion. Section one discusses the implications and limitations of our boiling regime classifications as this will define the interpretation of the results. Boiling regimes are dependent on heat transfer rates which in turn are subject to the fall conditions for each given cylinder which does not explicitly imply cylinder temperature. Section two will aim to quantify the stability of our initial observations using Euler angles. Euler angles describe any object orientation using a reference orientation. In this way we may understand the stability path of our object as it moves down the column [31].

4.1. Boiling regime classification

4.1.1. Terminal Velocity

When viewing the stability of a cylinder it is useful to understand the forces acting as it falls. The terminal velocity enlightens us to the forces acting in the vertical direction and is defined as the first instance the free-falling cylinder has zero acceleration i.e., $\frac{\delta(v_t)}{\delta t} = 0$. Equation (2) shows the general equation for any free-falling cylinder. F_g is the force associated with the gravitational acceleration, F_b is the force associated with the difference between an object's density and the medium in which it falls, and F_D is the force associated with friction and drag. Subscripts c ad v indicate that the forces are attributed to the cylinder and the vaporised Novec 7000 respectively. F_{VF} represents the forces due to vapour rectification over the body of the cylinder. In the case of a cylinder falling in the single-phase, $F_{VF} = 0$ and $\left(F_g - F_b\right)_v = 0$. We also assume that for smooth cylinders falling in the nucleate boiling and film boiling regimes $F_{VF} = 0$, giving

$$\left(F_g - F_b\right)_c + \left(F_g - F_b\right)_v - F_D + F_{VF} = 0 \ \#(2)$$

$$\left(F_g - F_b\right)_c + \left(F_g - F_b\right)_v - F_D = 0 \ \#(3)$$

rise to the general equation for a smooth free-falling cylinder and ratcheted cylinders falling within the single-phase. In the smooth case then, any lateral instability would be caused by pressure fluctuations in the wake behind the free-falling cylinder very much in line with the traditional approach of stability analysis whereby viscous action at the solid-liquid interfaces create eddies and is represented by F_D [28]. Similarly, for ratcheted cylinders falling within the single phase, drag force contributions would adequately describe free-fall instabilities. Now consider the opposite extreme, cylinders falling within the film boiling regime. Here two interfaces exist. The solid-vapour interface and the liquid-vapour interface. In this context skin friction is eliminated and if one views the free-fall of a smooth cylinder, one could say that instabilities arise because of form drag alone. Furthermore – the vapour layer absorbs surface difference, which implies that the form of a smooth cylinder is equal to that of a ratcheted cylinder (Figure A2 and Figure A3). Here then differences in stability between ratcheted cylinders and smooth cylinders would occur because of the vapour rectification represented by F_{VF} rather than F_D as in the single-phase case. The nucleate boiling regime introduces an altogether more complicated situation whereby lateral motion is some part of both drag force contributions and vapour rectifications. Furthermore, the complete image of lateral instability cannot be viewed by analysing the terminal velocity alone. The cavitation of bubbles at the surface of the free-falling cylinder induces with them a force, whereby the action of cavitating bubbles can both push and pull a cylinder.

4.1.2. Time taken to reach terminal velocity

The time taken to reach terminal velocity is an important factor to consider within boiling. Consider that our cylinders are heated only before they enter the column to free-fall. This means that the cylinders are constantly cooling as they fall, and the time taken before regime classification implies too the energy lost to the body of Novec 7000. Consider also that the different boiling regimes implies different heat transfer rates. For the experiments where cylinders are initially heated to 50℃ and remembering that Novec 7000 has a boiling point of 34℃, you would expect a significant amount of boiling to occur as the cylinders enter the column to fall. We do notice boiling in these experiments, but crucially not at the point of terminal velocity – this means the cylinders have all cooled to, or below, 34℃ by the time they reach their maximum velocity. Notice too that Figure 3a shows the only result where a smooth cylinder collides with the column wall during free-fall in isothermal conditions whereas in the nucleate boiling regime, 54% of cylinders heated up to 150℃ (Figure 4), result in collisions with the wall – 5% more than the next most unstable experiment which happens when the cylinders are initially heated to 50℃ (Figure 3). The instabilities due to random nucleate boiling action are clear. We accept that while nucleate boiling affects stability substantially, we aim to highlight that the mechanism of stability significantly differs with a lubricating layer of vapour, in so far as the stability of a cylinder depends more on skin friction factors in the single-phase regime, while in the film boiling regime vapour rectification becomes important.

4.1.3. Depth at which terminal velocity occurs

The depth at which terminal velocity occurs also holds significance when viewing the boiling regimes. Consider that vapour forms in two ways – through a temperature difference and a pressure difference. We understand that the boiling point of Novec 7000 in atmospheric pressure is 34℃; however, with a difference of 0.050 m below the surface, the surrounding pressure varies by an additional 686.7 Pa, which

implies that the boiling point of Novec 7000 varies also. Consider then Figure 3, and compare the depths of cylinders 2.0LD and SC2, which reach their terminal velocities at 0.582 m and 0.838 m respectively. One might feel compelled to assume that both 2.0LD and SC2 are below 34℃ as at terminal velocity – the single-phase regime was observed; however consider that the increased depth also increases the boiling point of Novec 7000. Without a well-defined phase diagram for Novec 7000, we cannot make accurate assumptions regarding the temperature of a cylinder based on boiling regimes alone.

4.1.4. Cylinder Temperature

Having the time of the fall, the mass of the cylinder, and the heat capacity, one can guess the evolution of the temperature of the cylinder and therefore discuss further the boiling regimes. Here we present a qualitative discussion about the thermal side of the cylinder as it is cooling down during the fall. Consider first the single-phase regime. Heat energy from the cylinder would be lost to the bulk fluid via conduction at the solid-liquid interface. Convective action caused by the motion of the cylinder would then accelerate cooling further by maintaining the maximum possible temperature gradient between the cylinder and the fluid. Observing nucleate boiling on the surface of the cylinder indicates that the temperature difference between the cylinder and the bulk fluid is significant, in so far as heated molecules of fluid gain enough energy for phase-change before the motion of the cylinder, and therefore convective action, forces too great a distance between the heated molecules and the cylinder. What separates nucleate boiling from film boiling is the regions in which boiling occurs. Nucleate boiling occurs only in specific zones, known as nucleation sites. On a given substrate, nucleation sites can trap molecules in so far as they are unable to escape before they gain sufficient energy for phase-change, while other zones on the substrate are not able to transfer the energy required for phase-change before the molecules move far enough away from the walls of the cylinder. In film boiling, phase-change is more distributed and occurs frequently enough over

the surface of the cylinder for vapourised bubbles to collide and coalesce forming a layer of vapour between the solid cylinder and the build liquid fluid. In nucleate boiling, bulk liquid is in direct contact with the solid cylinder, all be it to a lesser extent when compared to the single-phase case; however, the increased temperature difference, increases too the rate of heat transfer from the cylinder to the bulk fluid when compared to the single-phase case. Additionally, the vapourised bubbles of Novec 7000 also contribute to the convective action adding to the convective action caused by the motion of the cylinder. With this, for both the nucleate boiling and single-phase cases we assume the maximum temperature gradient possible i.e., cylinder temperature minus the fluid temperature which is constant at 25℃ ± 3℃ for all experiments. For film boiling experiments, there exists a vapour layer between the cylinder and the bulk fluid. Here conduction occurs at the solid-vapour interface from the cylinder wall to the vapourised Novec 7000 and then at the vapour-liquid interface from the vapourised Novec 7000 to the liquid Novec 7000. We assume that vapour remains at the boiling point of Novec 7000 and assume that convective action occurs within the liquid Novec 7000 such that it remains at 25℃ as discussed with the single-phase and nucleate boiling cases. Effectivity the vapour layer then acts as a wall separating the cylinder from the liquid Novec 7000 (Figure A2 and Figure A3). We may predict the heat transfer rate by calculating first the overall heat transfer coefficient and then applying the genera; heat transfer rate equation, $Q = UA\Delta T_{LM}$.

4.2. Quantifying stability

To quantify stability using Euler angles we must first define the reference orientation to which the angle relates. In this paper we say that the reference orientation is an upright cylinder i.e., the tip of the leading edge and the centre of the trailing end lies on the axis that describes the length of the column (Figure B3). We further define the length of the column as the y-axis and the width of the column as the x-axis. The

depth of the column, uncaptured by our camera angle is represented by the z-axis. We set the origin of each measurement at the CoV of the captured cylinder. We call the angle made between the cylinder and the x-axis angle α. The angle between the cylinder and the y-axis is angle β, and the angle between the cylinder and the z-axis is angle γ. A full explanation can be found in Appendix B and C.

4.3. Discussion

Table 6: Summary of experimental run completing for single-phase and film boiling results. The results have been normalised for comparison.

Initial Cylinder Temperature	SC1	SC2	2.2LD	11.4LD	2.2LU	11.4LU	2.0LD	2.0SD	2.0LU	2.0SU
25℃ (single-phase)	1.00	0.57	0.71	0.14	0.43	1.00	0.83	0.00	0.83	0.00
50℃ (nucleate boiling)	0.86	0.43	0.29	0.14	0.71	1.00	0.83	0.00	0.83	0.00
150℃ (nucleate boiling)	1.00	0.00	1.00	0.29	1.00	1.00	0.00	0.17	0.00	0.17
250℃ (nucleate boiling)	1.00	0.43	1.00	0.71	1.00	1.00	0.67	0.33	0.17	0.67
350℃ (film boiling)	1.00	0.00	1.00	0.43	1.00	1.00	0.00	0.67	0.50	1.00
450℃ (film boiling)	1.00	0.57	1.00	1.00	1.00	1.00	0.67	1.00	0.83	1.00
550℃ (film boiling)	1.00	0.86	1.00	1.00	1.00	1.00	1.00	0.83	1.00	1.00

4.3.1. Isothermal conditions (25℃)

Introducing ratchet structures introduces with them instability. Comparing lateral ratchet structures, we see that in isothermal conditions, upward facing ratchets result in fewer completed runs; however, as aspect ratio increases – this trend reverses (Table 6). Comparing laterally orientated ratcheted cylinders with aspect ratios 2.0 and 2.2 we notice a greater stability in the smaller aspect ratio; however, the reader is encouraged to consider the differences in design between these cylinders. 2.0LD and 2.0LU, weigh 4.2 N less than 2.2LD and 2.2LU. Additionally, the distance between the CoV and the CoM for 2.0LD and 2.0LU is 11.92 mm compared to 12.16 mm for 2.2LD and 2.2 LU implying the former pair is less stable than the latter pair [28]. The additional weight results in a difference in terminal velocity of 0.050 m/s.

$$C_d = \frac{Vg(\rho_c - \rho_f)}{0.5\pi\rho_f v_t r^2} \#(4)$$

Using equation (4), where V is volume, g is gravitational acceleration, ρ_c is the density of the cylinder, ρ_f is the density of the bulk fluid, v_t is the terminal velocity, r is the cylinder radius, and C_d is the drag coefficient, we see that the increase in terminal velocity results in a decrease in drag coefficient C_d of 0.1. When we compare the lateral orientation of the ratchet structures with the spiral orientation of the ratchet structures, we notice a remarkable difference with no completed runs for either upward or downward facing ratchets when spirally orientated.

4.3.2. Film boiling

The addition of vapour brings with it stability and the thicker the vapour layer the more stable the free-falls become. For an aspect ratio of 11.4, free-falls become as stable as if the cylinders were smooth. For aspect ratios of 2.0 and 2.2 we see that downward facing ratchets are the more unstable, reversing the trend seen in the isothermal case. Similarly, in comparing laterally oriented ratchets with spirally orientated ratchets we notice that spirally oriented ratchets complete more runs than laterally oriented ratchets – reversing the trend seen at isothermal conditions again. For the cylinders initially heated to 450℃ and 550℃ we propose that equation (3) can be used to define the drag force adequately as the vapour layer reduces the instabilities caused by the ratchet structures. For the cylinders initially heated to 350℃ we suggest that equation (2) must be used as describing the instability as using a drag force contribution alone under defines the system. We propose that the force associated with viscous friction must be included, as is the case with equation (2), to describe systems of three phases or more as the vapour rectification in our cases drastically change the outcome of the free-falls.

5. Conclusion

A purpose-built experimental rig investigates the influence of the Leidenfrost effect on the stability of

free-falling ratcheted cylinders. Ten cylinders were each released to fall freely in an extruded square tube filled with Novec 7000. To force cylinders to fall vertically – their Centre of Mass (CoM) was below their Centre of Volume (CoV), achieved by hollowing them out. To investigate aspect ratio we used a hollow 54% V/V and for our investigation of spirally oriented ratchets against laterally orientated ratchets we used a hollow of 56% V/V. In isothermal conditions, cylinders reached an average terminal velocity of 0.714 m/s, slowing down to 0.479 m/s and 0.365 m/s in the nucleate and film boiling regimes respectively. Smooth cylinders are significantly more stable than ratcheted cylinders across all boiling regimes achieving an overall completion rate of 98.98%. In isothermal conditions, for small ratchet ARs, downward facing ratchets result in greater stabilities with completion rates of 57% compared to completion rates of 14% for ratchets which are oriented upwards; however, as aspect ratio increases this result changes where upward facing ratchets are 29% more stable. Within isothermal conditions, orientating the ratchet structures so that they spiral upward along the length of the cylinder disrupts the stability when compared to orientating them laterally, with no completed runs for spirally orientated ratchets compared to an 83% completion rate for laterally orientated ratchets. The nucleate boiling regime is the most unstable situation for ratcheted and smooth cylinders. We propose that cavitating action pushes and pulls the cylinders in an unpredictable way. Introducing a vapour layer changes the stability of free-falling ratcheted cylinders but leaves smooth cylinders unaffected. Where downward facing ratchets increased stability in the single-phase regime, upward facing ratchets are 18% more stable in the film boiling regime. Similarly, where laterally orientated cylinders were more stable in the single-phase regime, spirally orientated cylinders become 25% more stable. As aspect ratio increases, film boiling eliminates instabilities associated with the ratchet structures. We propose that ratchet structures rectify the vapour flow within the vapour layer resulting in viscous drag forces that alter the stabilising action of free-falling cylinders. Additionally, we find that as the thickness of the vapour layer increases, the

influence of the ratchet structures decreases suggesting that there exists a limiting thickness to which vapour rectification remains relevant. We aim to quantify the instability of these viscous drag forces using 3D Euler angles which we achieve using a bespoke software tool.

Acknowledgments

This work was supported by the UK Engineering and Physical Sciences Research Council (EPSRC) for the University of Edinburgh Centre for Doctoral Training. The technicians primarily built the experimental apparatus at the University of Edinburgh, particularly Mr. S. Cummings, Mr. P. Aitken, and Mr. J. Graham. The aluminium cylinders used for the results presented herein were produced by George Brown & Sons Engineers Ltd.

Nomenclature

2.0LD Laterally orientated ratcheted cylinder with the flat side of the ratchets facing downward during free-fall and a ratchet aspect ratio (h/w) defined by 2.0, where h = 1.0 mm and w = 0.5mm

2.0LU Laterally orientated ratcheted cylinder with the flat side of the ratchets facing downward during free-fall and a ratchet aspect ratio (h/w) defined by 2.0, where h = 1.0 mm and w = 0.5mm

2.0SD Spirally orientated ratcheted cylinder with the flat side of the ratchets facing downward during free-fall and a ratchet aspect ratio (h/w) defined by 2.0, where h = 1.0 mm and w = 0.5mm

2.0SU Spirally orientated ratcheted cylinder with the flat side of the ratchets facing downward during free-fall and a ratchet aspect ratio (h/w) defined by 2.0, where h = 1.0 mm and w = 0.5mm

2.2LD Laterally orientated ratcheted cylinder with the flat side of the ratchets facing downward during free-fall and a ratchet aspect ratio (h/w) defined by 2.2, where h = 1.1 mm and w = 0.5mm

2.2LU Laterally orientated ratcheted cylinder with the flat side of the ratchets facing downward during free-fall and a ratchet aspect ratio (h/w) defined by 2.2, where h = 1.1 mm and w = 0.5mm

11.4LD Laterally orientated ratcheted cylinder with the flat side of the ratchets facing downward during free-fall and a ratchet aspect ratio (h/w) defined by 11.4, where h = 5.7 mm and w = 0.5mm

11.4LU Laterally orientated ratcheted cylinder with the flat side of the ratchets facing downward during free-fall and a ratchet aspect ratio (h/w) defined by 11.4, where h = 5.7 mm and w = 0.5mm

A Matrix associated with the rectangle found to represent the projected area of the cylinder

A' Rotated matrix associated with the projected area of the cylinder

Ap Projected area of the cylinder, m^2

AR Aspect Ratio

B	Matrix associated with the binary image using a threshold of 25.
D	The diameter of a smooth cylinder, excluding the length added by the ratchet widths, m
Ds	Maximum possible projected area of the cylinder, m^2
d	Diameter of the hollow within a free-falling cylinder, m
F	Force, N
fps	Frames per second
HSC	High-speed camera
h	Ratchet height or parallel length concerning the cylinder length of the engraved ratchets, m
L	The length of a cylinder, measured from the base of the cylinder to the base of the cone surmounted at the leading end, m
l	Depth of the hollow within a free-falling cylinder, m
P	The pitch of the surmounted cone, or height of the cone, m
Pl	Path length of free-falling cylinder, m
Px	Number of pixels within a matrix that is greater than zero to represent the projected area of a free-falling cylinder digitally.
r	Cylinder radius, m
SC1	Smooth cylinder used as a control for the investigation concerning the influence of aspect ratio

SC2	Smooth cylinder used as a control for the investigation concerning the influence of spiralled ratchet structures
t	Time, *s*
v	Velocity, m/s
V	Volume, m^3
w	Ratchet width or perpendicular length concerning the cylinder length of the engraved ratchets, m
x	Axis associated with the width of the column
y	Axis associated with the length of the column
z	Axis associated with the depth of the column

Greek Symbols

α	Angle of the cylinder to the x-axis
β	Angle of the cylinder to the y-axis
γ	Angle of the cylinder to the z-axis
ρ	Density, kg/m^3
σ	Absolute error

Subscripts

b	Buoyancy
c	Cylinder
D	Drag
f	Fluid
g	Gravity
Pl	Path length of free-falling cylinder, m
t	Terminal velocity
VF	As associated with the viscous friction force
v	*Vapour*

References

[1] J. G. Leidenfrost, "On the fixation of water in diverse fire," *Int. J. Heat Mass Transf.*, vol. 9, no. 11, pp. 1153–1166, 1966.

[2] J. T. Ok, J. Choi, E. Brown, and S. Park, "Effect of different fluids on rectified motion of Leidenfrost droplets on micro/sub-micron ratchets," *Microelectron. Eng.*, vol. 158, pp. 130–134, 2016, doi: 10.1016/j.mee.2016.04.018.

[3] S. D. Janssens, S. Koizumi, and E. Fried, "Behavior of self-propelled acetone droplets in a Leidenfrost state on liquid substrates," *Phys. Fluids*, vol. 29, no. 3, 2017, doi: 10.1063/1.4977442.

[4] G. Lagubeau, M. Le Merrer, C. Clanet, and D. Quéré, "Leidenfrost on a ratchet," *Nat. Phys.*, vol. 7, no. 5, pp. 395–398, 2011, doi: 10.1038/nphys1925.

[5] S. Diniega *et al.*, "A new dry hypothesis for the formation of martian linear gullies," *Icarus*, vol. 225, no. 1, pp. 526–537, 2013, doi: 10.1016/j.icarus.2013.04.006.

[6] A. L. Biance, C. Clanet, and D. Quéré, "Leidenfrost drops," *Phys. Fluids*, vol. 15, no. 6, pp. 1632–1637, 2003, doi: 10.1063/1.1572161.

[7] H. Linke *et al.*, "Self-propelled leidenfrost droplets," *Phys. Rev. Lett.*, vol. 96, no. 15, pp. 2–5, 2006, doi: 10.1103/PhysRevLett.96.154502.

[8] A. Bouillant, T. Mouterde, P. Bourrianne, A. Lagarde, C. Clanet, and D. Quéré, "Leidenfrost wheels," *Nat. Phys.*, vol. 14, no. 12, pp. 1188–1192, 2018, doi: 10.1038/s41567-018-0275-9.

[9] G. Dupeux, M. Le Merrer, G. Lagubeau, C. Clanet, S. Hardt, and D. Quéré, "Viscous mechanism for Leidenfrost propulsion on a ratchet," *Epl*, vol. 96, no. 5, 2011, doi: 10.1209/0295-5075/96/58001.

[10] M. Mrinal, X. Wang, and C. Luo, "Self-Rotation-Induced Propulsion of a Leidenfrost Drop on a Ratchet," *Langmuir*, vol. 33, no. 25, pp. 6307–6313, 2017, doi: 10.1021/acs.langmuir.7b01420.

[11] A. Würger, "Leidenfrost gas ratchets driven by thermal creep," *Phys. Rev. Lett.*, vol. 107, no. 16, pp. 1–4, 2011, doi: 10.1103/PhysRevLett.107.164502.

[12] D. Soto, G. Lagubeau, C. Clanet, and D. Quéré, "Surfing on a herringbone," *Phys. Rev. Fluids*, vol. 1, no. 1, pp. 1–10, 2016, doi: 10.1103/PhysRevFluids.1.013902.

[13] P. Agrawal *et al.*, "Leidenfrost heat engine: Sustained rotation of levitating rotors on turbine-inspired substrates," *Appl. Energy*, vol. 240, no. February, pp. 399–408, 2019, doi: 10.1016/j.apenergy.2019.02.034.

[14] G. Dupeux, T. Baier, V. Bacot, S. Hardt, C. Clanet, and D. Quéré, "Self-propelling uneven Leidenfrost solids," *Phys. Fluids*, vol. 25, no. 5, pp. 1–7, 2013, doi: 10.1063/1.4807007.

[15] T. R. Cousins, R. E. Goldstein, J. W. Jaworski, and A. I. Pesci, "A ratchet trap for Leidenfrost

drops," *J. Fluid Mech.*, vol. 696, pp. 215–227, 2012, doi: 10.1017/jfm.2012.27.

[16] R. L. Agapov *et al.*, "Length scale of Leidenfrost ratchet switches droplet directionality," *Nanoscale*, vol. 6, no. 15, pp. 9293–9299, 2014, doi: 10.1039/c4nr02362e.

[17] G. Duursma, R. Kennedy, K. Sefiane, and Y. Yu, "Leidenfrost Droplets on Microstructured Surfaces," *Heat Transf. Eng.*, vol. 37, no. 13–14, pp. 1190–1200, 2016, doi: 10.1080/01457632.2015.1112610.

[18] A. Hashmi *et al.*, "Leidenfrost levitation: Beyond droplets," *Sci. Rep.*, vol. 2, pp. 2–5, 2012, doi: 10.1038/srep00797.

[19] M. Shi, X. Ji, S. Feng, Q. Yang, T. J. Lu, and F. Xu, "Self-Propelled Hovercraft Based on Cold Leidenfrost Phenomenon," *Sci. Rep.*, vol. 6, pp. 1–7, 2016, doi: 10.1038/srep28574.

[20] G. G. Wells, R. Ledesma-Aguilar, G. McHale, and K. Sefiane, "A sublimation heat engine," *Nat. Commun.*, vol. 6, pp. 1–7, 2015, doi: 10.1038/ncomms7390.

[21] E. Kawakami and R. E. A. Arndt, "Investigation of the behavior of ventilated supercavities," The University of Minnesota, 2011.

[22] J. H. Spurk, "On the gas loss from ventilated supercavities," *Acta Mech.*, vol. 155, no. 3–4, pp. 125–135, 2002, doi: 10.1007/BF01176238.

[23] E. L. Amromin, "Challenging Problems on Ventilated Cavitation and Paths to Their Computational Solutions," *J. Mar. Sci. Appl.*, vol. 18, no. 3, pp. 260–270, 2019, doi: 10.1007/s11804-019-00100-x.

[24] J. Wang, B. Wang, and D. Chen, "Underwater drag reduction by gas," *Friction*, vol. 2, no. 4, pp. 295–309, 2014, doi: 10.1007/s40544-014-0070-2.

[25] S. Ashley, "Warp Drive Underwater," *Sci. Am.*, vol. 284, no. 5, pp. 70–79, 2001.

[26] I. U. Vakarelski, J. O. Marston, D. Y. C. Chan, and S. T. Thoroddsen, "Drag reduction by

leidenfrost vapor layers," *Phys. Rev. Lett.*, vol. 106, no. 21, pp. 3–6, 2011, doi: 10.1103/PhysRevLett.106.214501.

[27] G. Xiang, L. Birk, X. Yu, and H. Lu, "Numerical study on the trajectory of dropped cylindrical objects," *Ocean Eng.*, vol. 130, no. April 2016, pp. 1–9, 2017, doi: 10.1016/j.oceaneng.2016.11.060.

[28] P. C. Chu, A. Gilles, and C. Fan, "Experiment of falling cylinder through the water column," *Exp. Therm. Fluid Sci.*, vol. 29, no. 5, pp. 555–568, 2005, doi: 10.1016/j.expthermflusci.2004.08.001.

[29] W. B. Frank *et al.*, "Aluminum," *Ullmann's Encyclopedia of Industrial Chemistry*. Wiley-VCH Verlag GmbH & Co. KGaA, 2009, doi: 10.1002/14356007.a01_459.pub2.

[30] 3M, "3M™ Novec™ 7000 Engineered Fluid | Technical Data," 2021. [Online]. Available: https://multimedia.3m.com/mws/media/121372O/3m-novec-7000-engineered-fluid-tds.pdf.

[31] Q. Bai and M. Shehata, "Review study of using Euler angles and Euler parameters in multibody modeling of spatial holonomic and non-holonomic systems," *Int. J. Dyn. Control*, 2022, doi: 10.1007/s40435-022-00913-9.

List of Figure Captions

Notes on contributors

Adrian Jonas read Chemical Engineering at the University of Edinburgh, where he completed the integrated master's program in 2020. Adrian developed a passion for experimental research during his master's year, where he worked alongside Dr Anthony Buchoux and Prof Khellil Sefiane to develop a micro heat engine that uses the Leidenfrost effect for energy production. Adrian joined Prof K. Sefiane's research group in 2020, where he is currently studying towards a PhD at the University of Edinburgh.

Daniel Orejon (Dani) is a Senior Lecturer in Chemical Engineering at the Institute for Multiscale Thermofluids at the University of Edinburgh, WPI-I2CNER Associate Professor at Kyushu University (Japan), Associate Editor for the International Journal of Heat and Mass Transfer (Elsevier), and Fellow of the Higher Education Academy. Dani holds a 5-year bachelor's degree in Environmental and Industrial Chemical Engineering from the University of Seville (Spain) and PhD on the fundamentals of evaporation phase-change at the droplet scale from the Institute for Materials and Processes of the University of Edinburgh (UK)., In addition, Dani joined the International Institute for Carbon-Neutral Energy Research (WPI-I2CNER) at Kyushu University in Japan as a Post-Doctoral Research Associate for 3 years and as Assistant Professor for further 2 years. Dani additionally serves as School Postgraduate Progression Committee Representative for the Institute for Multiscale Thermofluids and as Teaching Laboratory Manager for the Chemical Engineering Discipline.

Khellil Sefiane, FRSC, FInstP, FJSPS, is a Professor of Thermophysical engineering at the University of Edinburgh (UoE), Assoc. Editor of Int. J. Heat and Mass Transfer, and RAEng ExxonMobil Fellow with more than 250 journal papers, and expert in novel experimental techniques for heat and mass transfer, phase change, moving contact lines, and flow regime transitions in mixtures. He has received the IoP Printing & Graphics Science Group Prize (2009) for his "Fundamental studies on droplet evaporation" as well as the Royal Academy of Engineering Global Research Award and elected the UK representative on the EUROTHERM Committee (http://www.eurothermcommittee.eu), member of the Scientific Council of the Int. Centre for Heat and Mass Transfer (http://www.ichmt.org/). Professor K. Sefiane has been an associate editor for the ASME Journal of Heat Transfer and the International Journal of Multiphase Flows."

Declaration of Competing Interest

☒ The authors declare that they have no known competing financial interests or personal relationships that could have appeared to influence the work reported in this paper.

Graphical abstract

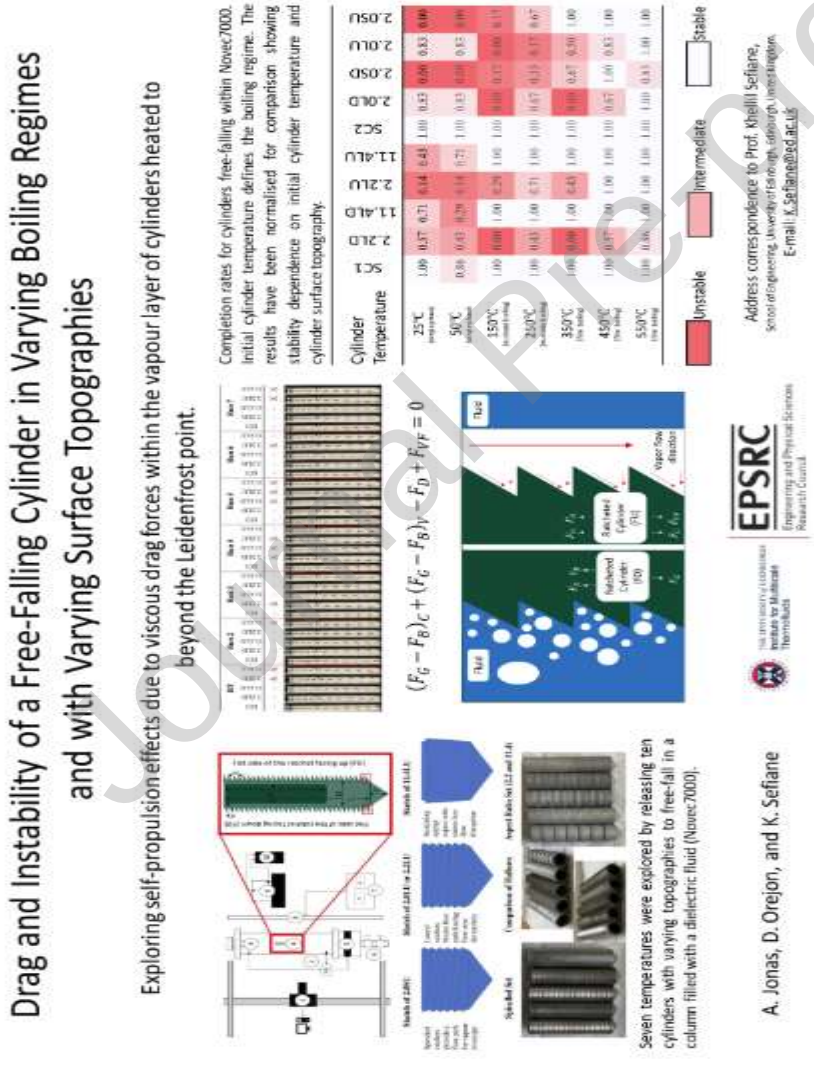

Highlights

- The stability of a cylinder is dependent on both temperature and surface topography.
- Smooth cylinders are 98% stable across all boiling regimes.
- Ratcheted cylinders are 42% stable under no boiling while film boiling increases stability by 39%.
- Nucleate boiling reduces stability by 5% for ratcheted cylinders.
- Ratcheted cylinders remain 57%, 88%, and 96% stable for initial temperatures of 350^{o}C, 450^{o}C, 550^{o}C respectively.